

Article

State-of-Charge Estimation of Batteries for Hybrid Urban Air Mobility

Min Young Yoo ¹, Jung Heon Lee ², Joo-Ho Choi ¹, Jae Sung Huh ³ and Woosuk Sung ^{4,*}

¹ School of Aerospace & Mechanical Engineering, Korea Aerospace University, Goyang-si 10540, Gyeonggi-do, Republic of Korea

² Department of Smart Air Mobility, Korea Aerospace University, Goyang-si 10540, Gyeonggi-do, Republic of Korea

³ Aerospace Propulsion Division, Korea Aerospace Research Institute, Yuseong-gu, Daejeon 34133, Republic of Korea

⁴ School of Mechanical System and Automotive Engineering, Chosun University, Gwangju 61452, Republic of Korea

* Correspondence: wsung@chosun.ac.kr

Abstract: This paper proposes a framework for accurately estimating the state-of-charge (SOC) and current sensor bias, with the aim of integrating it into urban air mobility (UAM) with hybrid propulsion. Considering the heightened safety concerns in an airborne environment, more reliable state estimation is required, particularly for the UAM that uses a battery as its primary power source. To ensure the suitability of the framework for the UAM, a two-pronged approach is taken. First, realistic test profiles, reflecting actual operational scenarios for the UAM, are used to model the battery and validate its state estimator. These profiles incorporate variations in battery power flow, namely, charge-depleting and charge-sustaining modes, during the different phases of the UAM's flight, including take-off, cruise, and landing. Moreover, the current sensor bias is estimated and corrected concurrently with the SOC. An extended Kalman filter-based bias estimator is developed and experimentally validated using actual current measurements from a Hall sensor, which is prone to noise. With this correction, a SOC estimation error is consistently maintained at 2% or lower, even during transitions between operational modes.

Keywords: lithium-ion battery; urban air mobility; charge-sustaining; equivalent circuit model; extended kalman filter; state-of-charge (SOC); current sensor bias



Citation: Yoo, M.Y.; Lee, J.H.; Choi, J.-H.; Huh, J.S.; Sung, W.

State-of-Charge Estimation of Batteries for Hybrid Urban Air Mobility. *Aerospace* **2023**, *10*, 550. <https://doi.org/10.3390/aerospace10060550>

Academic Editors: Wim J. C. Verhagen, Mihaela A. Mitici, Matteo Davide Lorenzo Dalla Vedova, Adam F. Abdin and Anne Barros

Received: 4 March 2023

Revised: 26 May 2023

Accepted: 30 May 2023

Published: 8 June 2023



Copyright: © 2023 by the authors. Licensee MDPI, Basel, Switzerland. This article is an open access article distributed under the terms and conditions of the Creative Commons Attribution (CC BY) license (<https://creativecommons.org/licenses/by/4.0/>).

1. Introduction

Lithium-ion batteries (LIBs) have undergone substantial advancements in recent times. The average energy density of LIB cells currently falls between 150 and 200 Wh/kg, and some energy-dense models have even surpassed 250 Wh/kg [1]. The power density of these cells has risen, now reaching over 1000 W/kg. The cost of these cells has decreased to a level below 150 \$/kWh [2]. Thanks to their enhanced performance metrics and reduced cost, the use of LIBs has expanded, including into the realm of air vehicles. The Velis Electro serves as a notable example, receiving the world's first type of certification for an electric aircraft from the European Union Aviation Safety Agency in June 2020 [3]. This aircraft is propelled solely by a 345 V, 24.8 kWh LIB pack. This pack is placed apart in the airframe and connected in parallel to ensure safety and provide redundancy in case of any faults (see Figure 1a) [4]. The implementation of a large LIB pack as a main power supply, especially in air vehicles, requires careful consideration of safety concerns. As the major safety concerns for LIBs, functional issues, such as partial or complete loss of capacity and power capabilities, pose the greatest threats, along with thermal issues. The consequences of a decrease in these capabilities are much more severe in air vehicles, making the accurate state estimation of LIBs crucial. To address this issue, the Velis Electro

continuously monitors the health of its LIB pack (see Figure 1b). The type of aircraft under consideration in this study is urban air mobility (UAM) based on electric vertical take-off and landing (eVTOL). The UAM will serve as a unique mode of transportation for people in urban areas, offering increased accessibility, reduced traffic congestion, improved air quality, increased safety, and enhanced efficiency. To bring this service to life, different eVTOL designs are being studied, including the vectored thrust, lift + cruise, and wingless multicopter. Regardless of the design chosen, the UAM is propelled by either all-electric or hybrid systems, which utilize a combination of LIBs and, in some cases, a gas turbine.

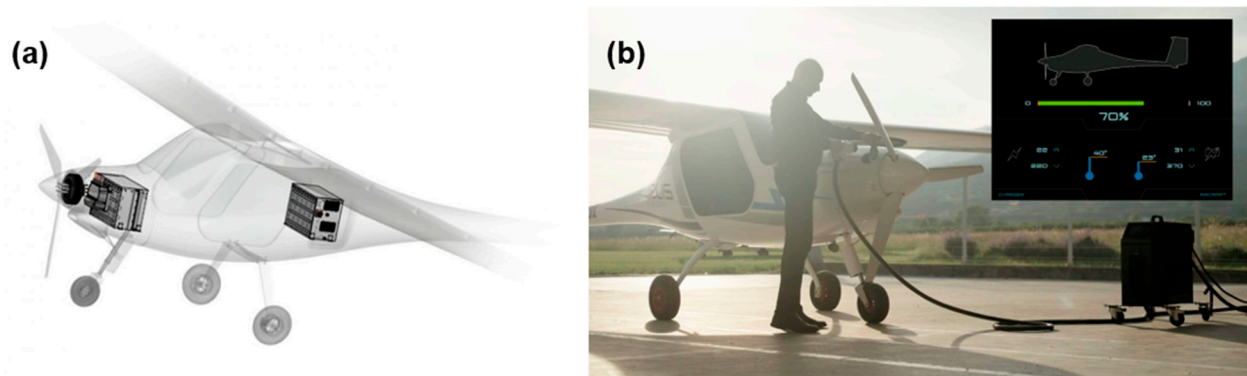


Figure 1. Velis Electro’s efforts to mitigate safety issues associated with LIBs: (a) redundant power supply and (b) accurate state estimation.

In light of the heightened safety concerns in an airborne environment, the accurate state estimation of LIBs is more important to a battery management system (BMS) for air vehicles such as UAMs. The state-of-charge (SOC) is one of the key states of LIBs, which refers to the amount of electrical energy remaining in the cell. An accurate SOC estimation is fundamental for the main functions of BMSs, involving cell balancing, charge-discharge control, and protection. An incorrect SOC estimation could lead to failure in power and energy management for electric aviation, with consequences that are far more severe than a car collision, including the worst-case scenario of a plane crash. Model-based SOC estimators are commonly used for improved accuracy and are frequently based on a combination of equivalent circuit models (ECMs) and Kalman filters (KFs).

Most SOC estimators have been developed and validated for pure electric vehicles that primarily operate in charge-depleting (CD) mode. However, there is an increasing demand for UAMs based on hybrid propulsion that can handle higher loads and longer distances, which involves transitions from CD to charge-sustaining (CS) mode. The hybrid system begins operating in CD mode for take-off and climbing. If the SOC reaches its lower limit, the mode switches to the CS. During cruising, the SOC is maintained by the gas turbine. If the SOC can be replenished during cruising, the mode switches back to the CD for descending and landing. The frequent switching between operational modes can make SOC estimation more difficult compared to when operating in the CD mode alone. Therefore, investigating SOC estimation in the CS mode is necessary for improved accuracy. A few studies have addressed this issue, but their focus is primarily on applications for ground vehicles, particularly plug-in hybrid electric vehicles (PHEVs) [5–7]. Mansour et al. [5] compared three adaptive filters, the particle filter (PF), extended Kalman filter (EKF), and unscented Kalman filter (UKF), to estimate the SOC in the CS mode. These filters were tuned using the noise covariance matching technique. They found that the PF provided the most accurate estimation, while both KFs were sufficiently robust to handle model uncertainty and simple to implement. Zhang et al. [6] developed a battery degradation model-based method to determine the optimal SOC for the CS mode. They found that the widely used 55% SOC was suboptimal for a LIB cell (SONY, 18650), and the corresponding best SOC was 37%, considering the potential estimation error. The former studies were conducted at the cell level, while the latter study was a system-level

approach incorporating major power components in a PHEV. Sohn et al. [7] proposed a power management strategy to maintain the SOC within the most efficient regime. They determined the target SOC for the CS control to be 52%, mainly considering the charge and discharge efficiency. The proposed strategy successfully maintained the average SOC between cells close to the target SOC over two test cycles, the urban dynamometer driving schedule (UDDS) and worldwide harmonized light-duty test cycle (WLTC) with three load powers, 300 W, 1 kW, and 2.5 kW.

Another difficulty arises from the current sensor bias. Model-based SOC estimators basically rely on Coulomb counting, which calculates the SOC by measuring the current flowing in or out of the cell, integrating the measurement over time, and dividing the integral by the total capacity. However, even if the initial SOC is known, this calculation is susceptible to bias in a current sensor and variations in the total capacity. Therefore, it is necessary to update the capacity fade and correct the bias to achieve an accurate SOC estimation. Our subsequent paper will address the issue of capacity estimation. Although many studies have discussed bias correction, the bias is generated by a hypothetical value that cannot be validated experimentally using actual readings from the current sensor [8–13]. Malysz et al. [8] proposed two methods to enhance filter performance, which involve estimating the deviations of model parameters and compensating for current bias. While they demonstrated the positive impact of bias correction on SOC estimation error, the magnitude of the injected bias (1000 mA) was not adequately justified. Zhao et al. [9] presented a method for estimating the SOC in the presence of sensor biases and emphasized the importance of observability analysis for selecting appropriate filters. They discovered that current bias had a lesser impact on filters' performance compared to voltage bias. Despite introducing a 100 mA bias in the current measurement, the first-order EKF achieved a SOC estimation with a root mean square error (RMSE) of 2.8%. They noted that the KFs were relatively robust against current sensor bias due to their knowledge of the OCV-SOC ground truth and model parameters, but the magnitude of the bias was not properly accounted for. Similarly [8], Al-Gabalawy et al. [10] identified two primary challenges to achieving dependable SOC estimation: varying model parameters and noisy and biased sensor measurements. To emulate this, they introduced Gaussian noise with a mean of zero and a standard deviation of 0.1% of the maximum value of the corresponding signal. The voltage and current bias were set at 20 mV and 12.5 mA, respectively. In a similar manner, Bhattacharyya et al. [11] added two constant values of current bias, 10 and 20 mA, to the current measurement and observed a reduction in SOC estimation accuracy with a mean absolute percentage error of 2.57% and 4.65%, respectively. However, it was not clear if these bias levels were reasonable in reality. He et al. [12] used the 5% bias-added current (slightly over 100 mA), which is also a hypothetical value with limited supporting evidence. Nevertheless, the suggested approach effectively mitigated the bias, resulting in a SOC error of less than 2%. The former studies were performed at the cell level, while the latter was a pack-level investigation. Nguyen Van et al. [12] employed a LIB pack to estimate the average SOC and current bias. The pack consists of seven modules connected in series, and each of the modules consists of nine cells connected in parallel, resulting in a total of 63 cells. Presumably accounting for the parallel connection between cells, they determined the magnitude of bias to be 500 mA, which is about five to fifty times higher than that reported in the cell-level studies. The proposed method estimated the bias with a maximum error of 0.1 A and a mean error of 4%.

This paper presents the development of our model-based SOC and current sensor bias estimator designed for use in the hybrid UAM. In order to effectively implement this estimator, it is crucial to obtain test data that reflects the battery's operating conditions. For ground vehicles, the test data can be easily obtained through common load profiles in the industry, but this approach is not yet applicable to the UAM due to its relatively early stage of development. To overcome this challenge, the test profiles are sourced from PHEVs which share similarities with the UAM in terms of their operational mode switching from CD to CS. When validating the SOC estimates against the test profile, a Hall sensor, the

most widely used type of current sensor for ground vehicles, is employed to generate the bias. The bias estimates are experimentally validated against actual readings from the shunt resistor, which features a higher degree of accuracy compared to the Hall sensor.

2. Prior Studies on Model-Based State Estimation

This section provides an overview of previous studies on model-based state estimation, with a focus on the battery models, state estimators, and test profiles used to estimate the SOC and current sensor bias. The SOC is expressed as the ratio of the residual capacity to the total capacity of the cell. The two underlying methods for estimating the SOC are based on either the cell voltage or current. The voltage-based method determines the SOC by measuring the terminal voltage of the cell and referencing a table that relates SOC to open-circuit voltage (OCV). However, this method can be influenced by the degree of polarization, which is the deviation of the terminal voltage from OCV with the passage of current. The current-based method calculates the SOC by measuring the current flowing into or out of the cell, integrating the measurement over time, and dividing the integral by the total capacity of the cell. However, even if the initial SOC is known, this method can be affected by the bias in the current sensor and variations in total capacity. The model-based method is an alternative approach that merges the benefits of both methods. This method utilizes model-based state estimators to deduce the internal state of a physical system based on sensor measurements. In the context of SOC estimation, this method entails passing the same current through both a physical cell and its virtual model and comparing the resulting measured and predicted voltages. An error between these voltages is used to estimate the SOC. However, it is crucial to make a careful correction as the error may result from inaccuracies not only in state estimates but also in measurements and a model. The current sensor bias, as previously noted, serves as a typical source of process noise in a model and continues to pose a challenge for achieving an accurate SOC estimation, despite the implementation of a model-based method.

Table 1. Prior studies on model-based SOC and/or current sensor bias estimator for ground vehicles.

Ref.	Battery Model	State Estimator	Test Profile	Range of SOC [%]	Amount of Bias [mA]	Notes
[5]	Thevenin	AEKF, AUKF, PF	-	30–50	-	Adaptive EKF, Adaptive UKF
[8]	Thevenin	KF, EKF	-	0–100	1000	
[9]	Thevenin	EKF, UKF	FUDS, Artemis	50~90	100	
[10]	Thevenin	KF, EKF, DEKF	-	40~100	12.5, 25	Dual EKF
[11]	Thevenin	EKF, DEKF	UDDS, NYCC, BCDC	10~100	10, 20	
[12]	Thevenin	AEKF	UDDS, HWFET, SFTP, NYCC, LA92 (combined)	0–100	113.5	Adaptive EKF
[13]	ESC	UKF	-	-	500	
[14]	Combined, Simple, Hysteresis, ESC	EKF	UDDS	10~90	-	
[15]	Rint, RC, Thevenin, PNGV	EKF	HPPC, DST, FUDS	20~100	-	
[16]	Thevenin, ESC	EKF, SVSF	UDDS	10~100	-	Smooth variable structure filter
[17]	Thevenin	EKF, UKF, ASRUKF	Constant, Pulse, DST	40~100	-	Adaptive square root UKF

Table 1. Cont.

Ref.	Battery Model	State Estimator	Test Profile	Range of SOC [%]	Amount of Bias [mA]	Notes
[18]	Thevenin	LPVS	Asymmetrical pulse	10~90	-	Linear parameter varying system
[19]	PNGV	EKF	HPPC	10~80	-	
[20]	PNGV	AEKF	HPPC	-	-	Adaptive EKF
[21]	ESC	EKF, MMAE, MMAE + EKF	Constant	0~100	-	Multiple model adaptive estimation
[22]	RC	SMO	Random current	0~100	-	
[23]	Thevenin	KF	Random current	10~100	-	
[24]	Thevenin	KF, EKF	Constant	10~100	-	
[25]	Thevenin	EKF, AUKF	UDDS, FTP, HWFET, NEDC, NYCC	0~100	-	Adaptive UKF
[26]	Thevenin	HEKF	DST, NEDC, FUDS	10~100	-	H-infinity UKF
[27]	RC	ALO	FUDS	10~90	-	Adaptive LO
[28]	Thevenin	PF	Pulse	10~100	-	
[29]	RC, Thevenin	AGSMO	UDDS	50~100	-	Adaptive gain SMO

Among possible options in the model-based method, ECMs combined with KFs have been widely used. This combination is especially suitable for real-time estimation using computationally light BMSs because ECMs can offer an efficient representation of battery behavior, and KFs can provide a robust solution for estimating battery states, even in the presence of measurement noise and model uncertainty. Numerous ECMs have been studied for their different levels of complexity and accuracy, including the Thevenin [5,8–12,15–18,23–26,28,29], RC [15,22,27,29], partnership for a new generation of vehicles (PNGV) [15,19,20], and enhanced self-correcting (ESC) [13,14,16,21]. In the pursuit of more reliable SOC estimation, various adaptive filters have been integrated with ECMs, such as the KF [8,23,24], EKF [5,7–11,13–17,19–21,24–26], UKF [5,9,12,17,25], PF [5,28], sliding mode observer (SMO) [22,29], and Luenberger observer (LO) [27]. Of particular interest are non-linear KFs [8–13], which have also been studied for their effectiveness in estimating the current sensor bias along with the SOC. Test data is required for both identifying model parameters and validating state estimates. To this end, various test profiles have been employed, such as the UDDS [11,13,14,16,25,29], federal urban dynamic schedule (FUDS) [9,15,26,27], highway fuel economy driving schedule (HWFET) [13,25], US06 supplemental federal test procedure (SFTP) [13], New York City cycle (NYCC) [11,13,25], LA92 [13], new European driving cycle (NEDC) [25,26], Artemis [9], Braunschweig city driving cycle (BCDC) [11], dynamic stress test (DST) [15,17,26], pulse tests such as hybrid pulse power characterization (HPPC) [15,19,20], and a test to charge and discharge with the same current [17,21,24]. An overview of notable prior studies on estimating the SOC and current sensor bias is provided in Table 1, which categorizes them according to the type of test profiles, state estimators, and battery models used.

3. LIB Cell Testing

This section details our experimental setup for generating test data.

3.1. Test Profile

Our load profile needs to incorporate the operational modes evolving from CD to CS, as the flight phase of the hybrid UAM progresses from take-off to cruise. However, previous studies have only concentrated on load profiles that are close to the CD mode. Since a load profile for the UAM has not been established yet, data from the D-segment PHEV was adopted as a preliminary study. Similar to the UAM, the hybrid system in the PHEV initially operates in the CD mode solely using the battery at its upper limit of the SOC. When the SOC decreases to its lower limit, the mode switches to the CS,

where the battery is replenished by a gasoline engine to maintain the SOC within a specific range. Figure 2 depicts an analogy between the operational modes of the hybrid UAM and PHEV. In order to diversify the characteristics of test data, three distinct load profiles were adopted: City, Highway, and High-speed. As their names indicate, the city profile is the least aggressive, while the High-speed profile is the most intense. As shown in Figure 3, the difference in characteristics is reflected in the magnitude and direction of the current, where positive values indicate battery discharge. The measured voltage is used as test data in the subsequent section. As noted, these load profiles were originally applied to a large LIB pack in the PHEV containing 96 cells, each with a nominal capacity of approximately 37 Ah. The magnitude of the current was scaled based on the C-rate to match with a smaller LIB cell used in this study. Except for the High-speed profile, the CD to CS mode transition in the City and Highway profiles occurs at approximately 15% SOC, which corresponds to 8500 s and 4300 s, respectively. The mode shift can also be noticed with a variation in the rate of change in the voltage.

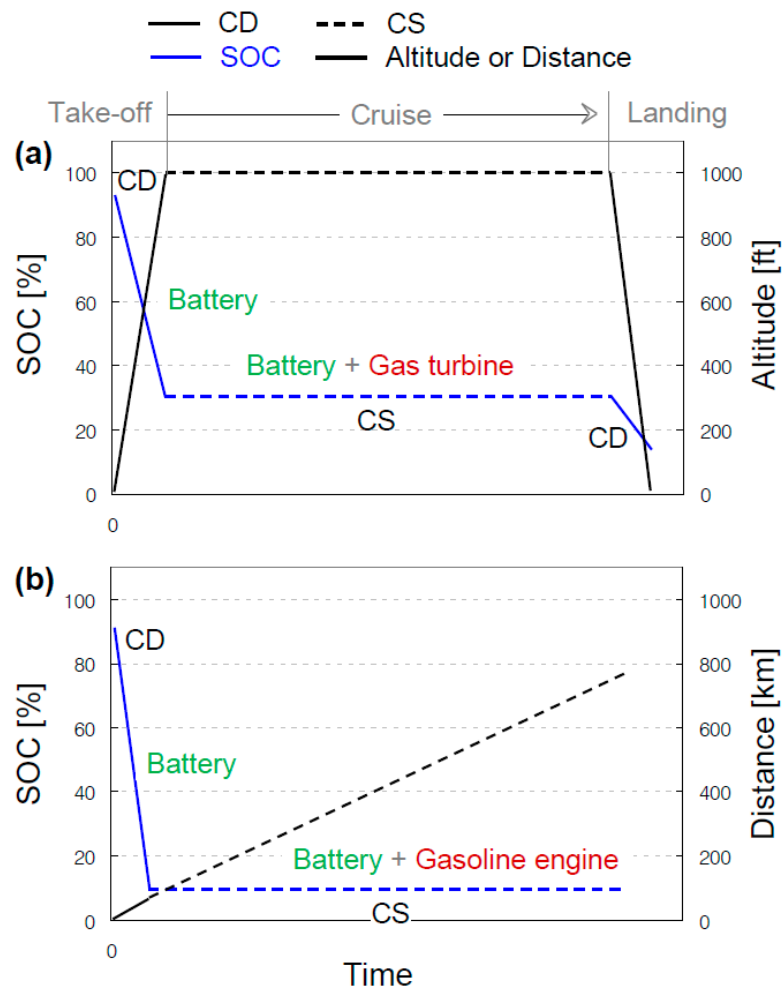


Figure 2. Similarity of the operational modes between (a) hybrid UAM and (b) PHEV.

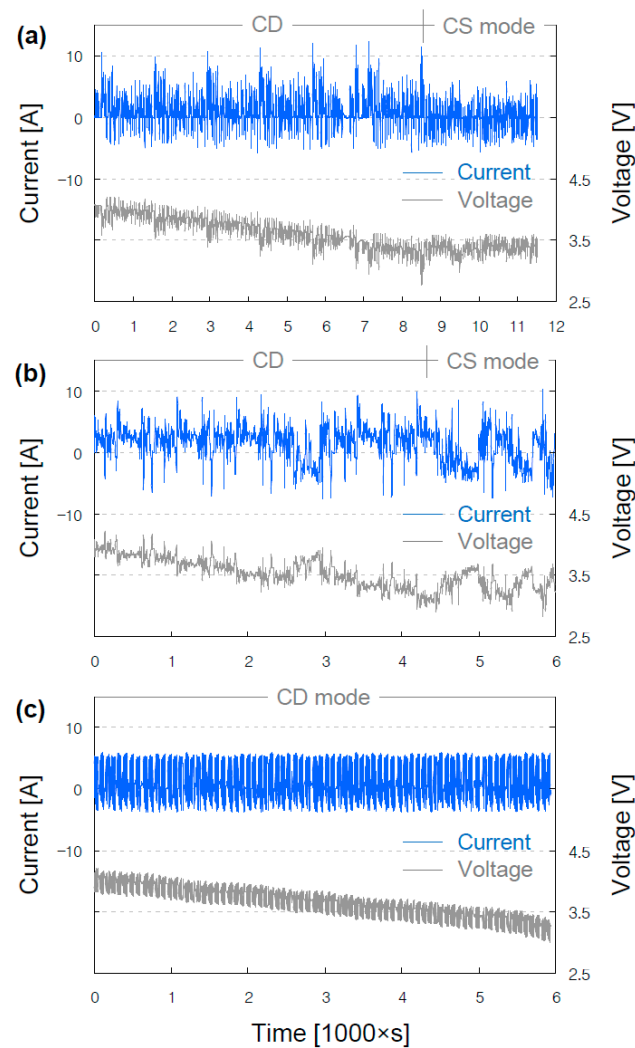


Figure 3. Voltage response to the current profiles adopted: (a) City, (b) Highway, and (c) High-speed.

3.2. Experiment Setup

In this study, a LIB cell (Samsung SDI, 18650-35E) with a nominal capacity of 3.5 Ah and a nominal voltage of 3.7 V was selected. The load profiles were simulated using the combination of a DC electronic load (Kikusui, PLZ1004W) and a DC power supply (Kikusui, PWR800L). The seamless transition between charge and discharge in the load profiles was facilitated by integrating these two pieces of equipment with a charge-discharge system controller (Kikusui, PFX2512) (see Figure 4). Apart from the current sensor built into the equipment, two additions were employed for cross-checking purposes: a hall sensor (LEM, DHAB S/145) and a shunt resistor (YOKOGAWA, 2215-09) (see Table 2). The latter uses direct measurement of the flow of current, which is proportional to the voltage drop across the shunt resistor within a circuit. On the other hand, the former uses indirect measurement of the magnetic field generated by the current flowing through a circuit. Each method has its advantages and disadvantages that are tied to the underlying physics of its measurement principles. When accuracy is a top priority, shunt resistors have a clear advantage as they rely on direct measurement. Despite having documented accuracy specifications, it is challenging to determine the actual measurement error of a non-contact Hall sensor due to the potential effects of various external influences. This indicates that Hall sensors tend to be susceptible to noise and are prone to bias. In contrast, Hall sensors are more compact, making them a good choice for applications where size minimization is important. This is particularly serious in high currents because a shunt resistor would have a footprint directly proportional to the magnitude of the current being measured. Taken together, a

Hall sensor can surpass shunt resistors, as long as its bias is effectively compensated. The accuracy of the current measurement can be evaluated with sensitivity. The Hall sensor used in this study, with a sensitivity of 10 mV/A, was four times inferior to the shunt resistor’s 2.5 mV/A resolution. In the following section, the effect of this difference on the accuracy of SOC estimation is experimentally demonstrated. Furthermore, the effect of this difference is minimized by correcting the bias in the Hall sensor while estimating the SOC.

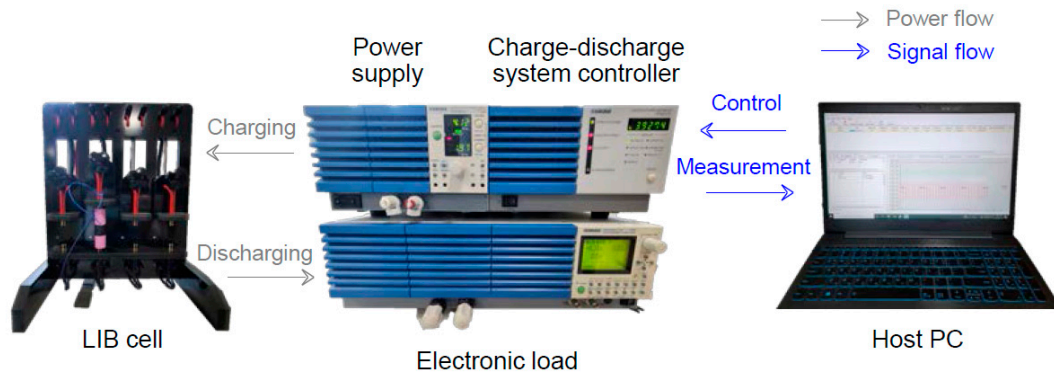
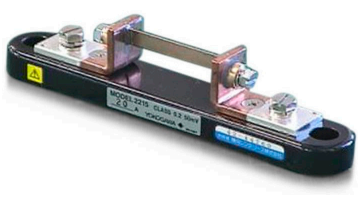


Figure 4. Experimental setup.

Table 2. Comparison of the current sensors utilized.

	Hall Sensor	Shunt Resistor
Model	LEM DHAB S/145	YOKOGAWA 2215-09
Input	200 A (Channel 2)	20 A
Output	2 V	50 mV
Sensitivity	10 mV/A	2.5 mV/A
Accuracy	3.3%	0.2%
Retail Price	\$35/ea	\$150/ea
Dimension (L × W × H)	52.75 × 48.5 × 24 mm	700 × 310 × 390 mm
Externals		
Ref.	[30]	[31]

3.3. Test Data

With the equipment in place, test data was collected through static and dynamic tests. The static test aims to establish the OCV-SOC relationship of the cell. The dynamic test aims to identify the transient behavior of the cell against the applied load profiles. Figure 3 (dynamic test) and Figure 5 (static test) plot the test data generated. For a feasibility study, test data based on the city profile was used to calculate the SOC simply by Coulomb counting with the two current sensors being compared. The results are in Figure 6. The Hall sensor’s output indicates that even a slight variance in current measurement can accumulate and lead to a notable difference in the estimation of SOC. The shunt resistor’s output indicates that the operational mode transition takes place at 15% SOC, owing to its higher level of accuracy. Therefore, the bias in a Hall sensor needs to be estimated and corrected to accurately estimate the SOC.

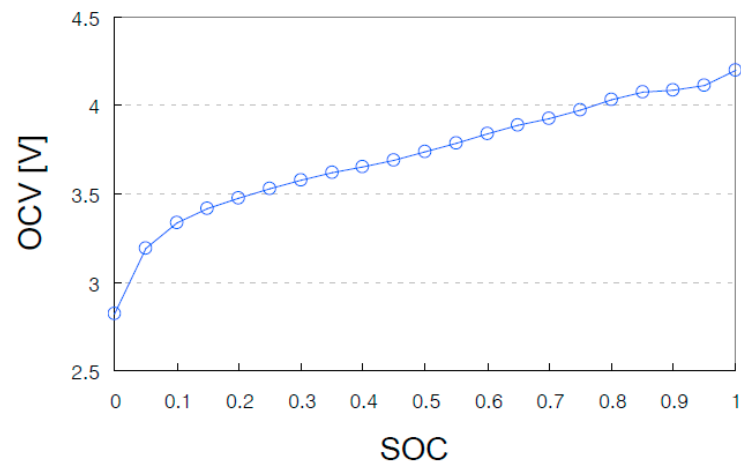


Figure 5. OCV-SOC relationship established.

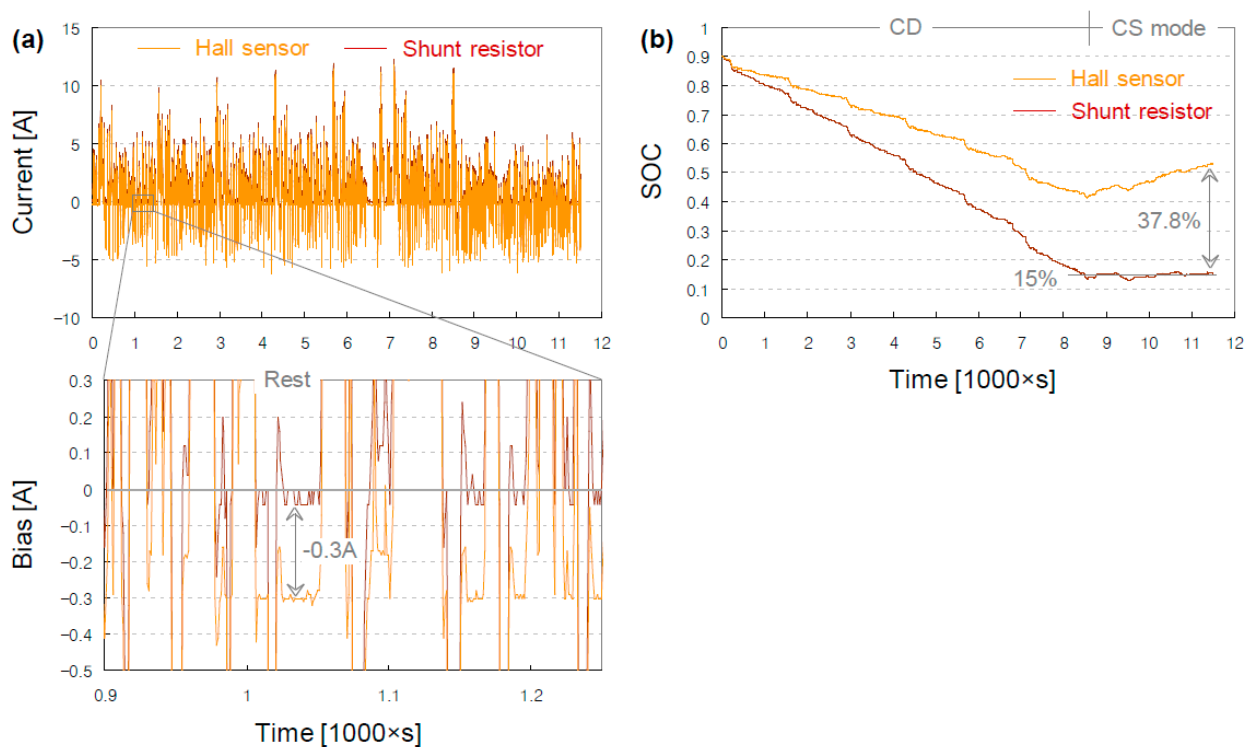


Figure 6. (a) Current sensor bias demonstrated during the city profile, (b) which affects the accuracy of SOC estimation.

4. Framework for Model-Based State Estimation

This section outlines the framework for accurately estimating the SOC and current sensor bias that comprises three major stages (see Table 3). The first stage is to generate test data (Stages 1.1 and 1.2). As in the previous section, the OCV-SOC relationship, as well as the voltage response to the current profile, were generated from the cell. In this study, the City, Highway, and High-speed profiles were applied to simulate the loads the cell may bear during actual operational scenarios for the UAM. The load profile's current input was monitored by the Hall sensor and shunt resistor.

Table 3. Three stages for estimating the SOC and current sensor bias.

Stage	Task	Output
1.1	Dynamic test	v_T
1.2	Static test	v_{OC}
2.1	Model formulation	$\hat{v}_T = v_{OC} + M_0s + Mh - R_0i - R_1i_{R_1} - R_2i_{R_2}$
2.2	Model parameter identification	$\tau_j, M, M_0, R_0, R_j, \gamma$
3.1	Filter parameter tuning	$\Sigma_z, \Sigma_{i_b}, \Sigma_v, \Sigma_\omega$
3.2	State estimation	i_R, z, h, i_b

The next stage is to formulate the cell model and identify its parameters (Stages 2.1 and 2.2). This study exploited the Thevenin and ESC models. The Thevenin model is considered the most representative form of ECMs. This model captures the time-varying polarization voltages simply using one or more parallel resistor-capacitor elements. The ESC model is an advanced form of the Thevenin model. As shown in Figure 7, this model captures the SOC-varying and instantaneous hysteresis voltages using an additional element connected in series to the R-C elements. These models were developed using an evolutionary approach, allowing for the gradual incorporation of relevant model states to more accurately predict the cell’s transient behavior. Overall, the output v_T (terminal voltage) is predicted in response to the input i (current flowing through R_0 (ohmic resistance)). The Thevenin model to estimate the SOC is formed by first incorporating the states, i_{R_j} (current flowing through R_j and C_j (polarization resistance and capacitance) and z (SOC)). Then, the state i_b (current bias) is added to the input i to account for the current sensor bias. Finally, the addition of the state h (hysteresis voltage) and input s (instantaneous hysteresis voltage) completes the ESC model. The resulting non-linear system model and measurement function of the ESC model are described separately in Appendix A for the sake of brevity.

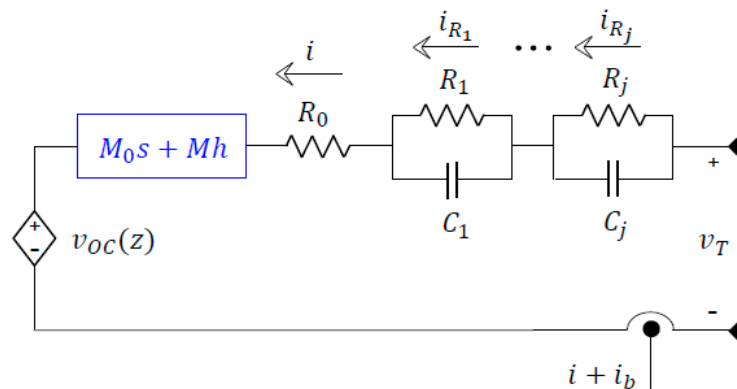


Figure 7. Circuit schematic for the ESC model that is nearly identical to that of the Thevenin model, except for the inclusion of hysteresis voltages (in blue).

The optimization of parameters in the formulated models was divided into a series of steps, rather than identifying all parameters at once. The cell’s Coulombic efficiency and total capacity are first determined from the test data and specification sheet, respectively. Subsequently, subspace system identification (a suboptimal linear optimization method) [32,33] is utilized to directly solve for R_jC_j (time constants τ_j), avoiding many of the challenges associated with non-linear optimization, such as local minima, slow convergence, and high sensitivity to an initial guess. Using the initial guess of γ (the decay rate of hysteresis), i_{R_j} , z , h , s and OCV are then computed. The remaining M (maximum hysteresis), M_0 (maximum instantaneous hysteresis), R_0 and R_j are iteratively solved using a non-negative least square method [34] that minimizes the difference between the measured and predicted voltages. Finally, the γ is updated with the same method.

The final stage is to estimate the SOC and current sensor bias (Stages 3.1 and 3.2). This study applied the EKF to the parameterized models. Basically, the KF is a recursive

approach that repeatedly updates the state estimates of the system at each time step based on the new measurements. Details regarding the estimation steps can be found in [35]. The KF assumes that the system model and measurement function are linear, but these functions in the ESC model are non-linear. The Taylor series expansion was used to analytically obtain a linear approximation of these non-linear functions, allowing the states to be estimated using the EKF. The linearized system model and measurement function of the ESC model are succinctly presented in Appendix A through the use of matrix-vector multiplication.

5. Results

This section evaluates the performance of the model-based SOC and current sensor bias estimator.

5.1. Model Parameters Identification

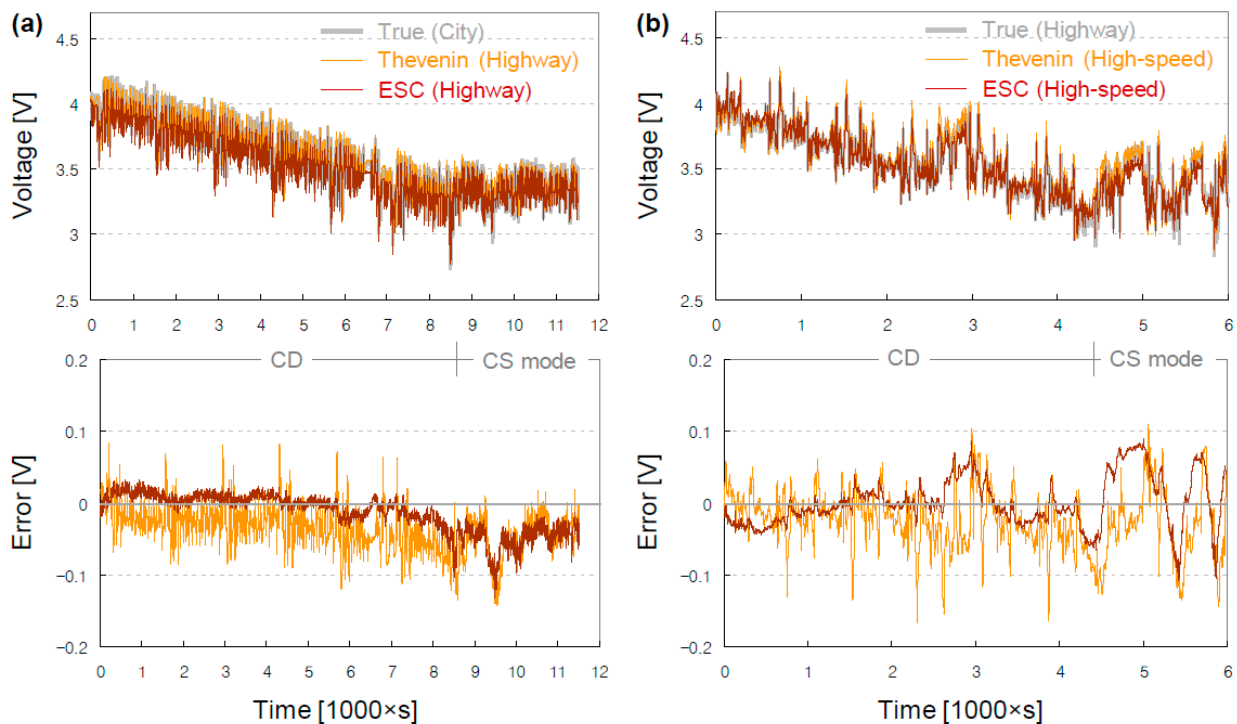
In accordance with the framework outlined in the preceding section, six models were constructed by applying the three load profiles to the two cell models. These models are named after the load profile used for modeling. For instance, either Thevenin or ESC model based on the City profile is called the City model hereinafter. The results are presented in Table 4. It is noted that the hysteresis voltage parameters are only available for the ESC model. The uniformity of the polarization voltage parameters for the same load profile is a result of subspace system identification employed to directly solve for $R_j C_j$ before iteratively solving for other parameters. Table 5 lists the resulting RMSEs of the predicted terminal voltages for each load profile, cell model, and operational mode. It is noted that the CS mode is unavailable for the High-speed profile. Figure 8 plots the measured and predicted voltages along with their error, comparing modeling accuracy across the operational modes. Due to space constraints, it is difficult to plot all cases. Instead, the worst RMSE case was selected for each load profile, which are (a) the Highway model validated with the City profile and (b) the High-speed model tested using the Highway profile. The results indicate that the ESC model generally outperforms the Thevenin model in terminal voltage prediction. In both models, their error increases as the mode shifts from CD to CS, as was noted in Table 5. The reason is due to limitations in representing battery behavior at low SOCs, around 15%. However, this tendency is less severe in the ESC model. Although the error pattern of the two models looks similar in the CS mode, as shown in lower Figure 8, greater accuracy is obtained by the ESC model as a consequence of the inclusion of the hysteresis voltage state and its parameter. The results also demonstrate that a load profile used for modeling has no significant impact on modeling accuracy. That is, the High-speed models (CD mode only) exhibit comparable RMSEs to those produced by other models (CD and CS modes).

Table 4. Comparison of model parameters identified.

		Ohmic	Polarization		Hysteresis Parameters		
		R_0 [ohm]	$R_1 C_1$ [s]	$R_2 C_2$ [s]	M [mV]	M_0 [mV]	γ
City	Thevenin	0.0401	1.2148	14.4792	-	-	-
	ESC	0.0396	1.2148	14.4792	109.5078	0	2.0179
Highway	Thevenin	0.0379	0.6056	9.2996	-	-	-
	ESC	0.0397	0.6056	9.2996	91.0749	4.292	29.2975
High-speed	Thevenin	0.0404	0.3567	8.1987	-	-	-
	ESC	0.0394	0.3567	8.1987	114.2882	0	2.5376

Table 5. Effect of cell modeling on the accuracy of terminal voltage prediction.

		RMSEs [mV]						
		CD	City CS	Overall	CD	Highway CS	Overall	High-Speed CD
City	Thevenin	37.96	54.69	42.98	34.32	56	42.79	27.54
	ESC	11.3	26.14	16.54	19.6	45.23	30.63	11.68
Highway	Thevenin	42.49	55.95	46.4	38.87	59.28	46.68	34.93
	ESC	14.96	48.67	28.04	15.63	31.37	22.16	14.99
High-speed	Thevenin	43.78	56.44	47.42	40.73	60.94	48.42	35.6
	ESC	13.14	27.87	18.19	24.02	51.24	35.5	12.83

**Figure 8.** Validation of terminal voltage prediction using the (a) City and (b) Highway profiles.

5.2. SOC Estimation

The EKF was utilized to estimate the SOC by the two cell models across the three load profiles. In the implementation, initial values of error variances w_{k-1} and v_k as shown in (A1) and (A2) in Appendix A should be assigned, which are the process and measurement noises, respectively. In this study, they were assigned with $w_0 = [1e-6, 1e-6, 0.01, 1e-8, 0.2]$, and $v_1 = 0.2$. Table 6 lists the resultant RMSEs of the estimated SOC for the two load profiles, City and Highway, by the six models constructed by the three load profiles and two cell models. It is noted that the High-speed profile is excluded from this comparison due to the absence of the CS mode. Figure 9 presents the results using a histogram, facilitating a comparison of estimation accuracy, in which the Thevenin and ESC models are distinguished by the edge colors orange and red. The results show that the ESC model consistently outperforms the Thevenin model in SOC estimation mainly due to its greater terminal voltage prediction accuracy. The results also show that the RMSEs of the High-speed model (green face color), which is constructed by the CD mode profile only, are of similar magnitude to the other two models: City (blue) and Highway (brown) constructed by the CD-CS mode profiles. This means that a load profile in the modeling has a negligible effect on estimation accuracy, which was contrary to our expectations.

Table 6. Effect of cell modeling on the accuracy of SOC estimation.

		RMSEs [%]					
		City			Highway		
		CD	CS	Overall	CD	CS	Overall
City	Thevenin	1.975	1.665	1.899	2.344	1.498	2.021
	ESC	1.732	0.56	1.515	1.253	1.123	1.34
Highway	Thevenin	2.492	1.85	2.341	2.208	2.101	2.173
	ESC	1.231	1.751	1.412	1.534	1.036	1.388
High-speed	Thevenin	2.344	1.804	2.215	2.768	1.946	2.237
	ESC	1.861	0.521	1.621	1.897	1.094	1.914

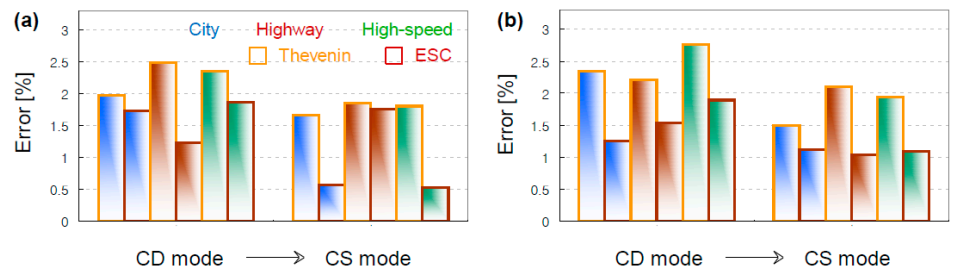


Figure 9. Evaluation of SOC estimation accuracy with cell modeling under the (a) City and (b) Highway profiles.

As a further comparison, the true and estimated SOC_s are plotted in Figure 10, along with their error for the six models. In the result, the true SOC was obtained by Coulomb counting of the current from the shunt resistor, while the estimated SOC was obtained by the EKF with bias correction from the Hall sensor.

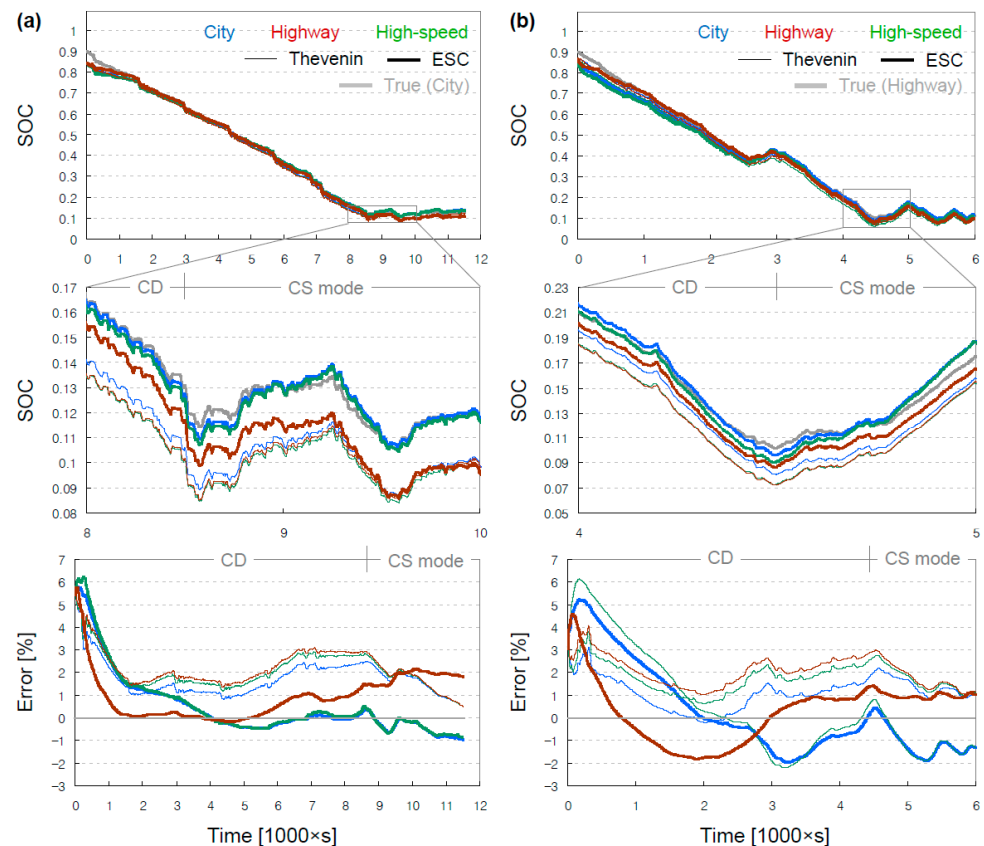


Figure 10. Validation of SOC estimation using the (a) City and (b) Highway profiles.

5.3. Current Sensor Bias Correction

The EKF was also utilized to estimate the current sensor bias. Table 7 lists the resulting RMSEs of the estimated SOCs, distinguishing between the results that were bias-corrected or not. Figure 11 presents the results using a histogram, facilitating a comparison of estimation accuracy. Figure 12 plots the true and estimated SOCs along with their error. Given its superiority over the Thevenin, it is noted that the ESC is the only model addressed in bias correction. In the last figures of Figure 12, the true and estimated biases are also plotted, in which the true value was obtained by the shunt resistor. In the results of City and Highway profiles, the true biases were measured to be approximately -0.38 A and -0.43 A, respectively. This indicates that the readings from the Hall sensor were approximately 0.4 A lower than those from the shunt resistor, which causes poor accuracy in SOC estimation; that is, the RMSE of SOC increases by nearly 6%, depending on load profiles used for modeling and validation. By correcting the bias, the RMSE is reduced to around 1%. In case the High-speed model is applied to the City profile, the RMSE of bias estimation between 2000 s and 11500 s is less than 0.05 A. The correction is less effective in the Highway profile, yielding a bias estimation RMSE of about 0.17 A between 2000 s and 6000 s.

Table 7. Effect of bias correction on the accuracy of SOC estimation.

		RMSEs [%]					
		CD	City CS	Overall	CD	Highway CS	Overall
City	Uncorrected	5.469	9.307	6.692	3.207	5.71	4.21
	Bias-corrected	1.732	0.56	1.515	1.253	1.123	1.34
Highway	Uncorrected	5.594	7.933	6.292	3.252	5.379	4.086
	Bias-corrected	1.231	1.751	1.412	1.534	1.036	1.388
High-speed	Uncorrected	5.574	9.427	6.79	3.441	5.581	4.275
	Bias-corrected	1.861	0.521	1.621	1.897	1.094	1.914

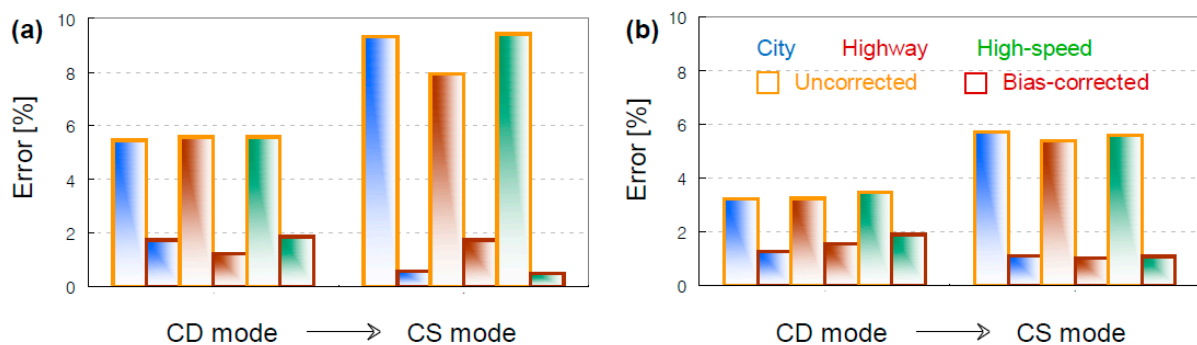


Figure 11. Evaluation of SOC estimation accuracy with bias correction under the (a) City and (b) Highway profiles.

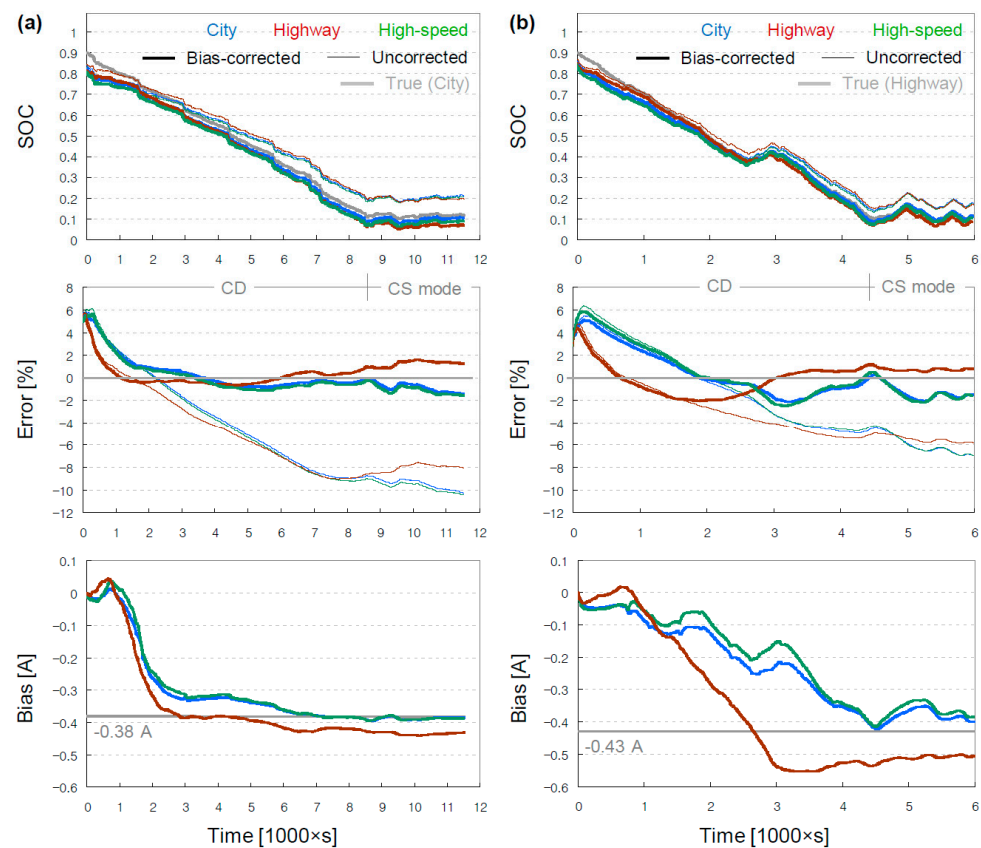


Figure 12. Validation of bias estimation using the (a) City and (b) Highway profiles.

6. Conclusions

This paper presented a framework for accurately estimating the SOC and current sensor bias, with the aim of applying it to UAMs with hybrid propulsion. Two main contributions of our study are summarized as follows: (1) For improved accuracy, realistic test profiles that simulate actual operational scenarios for the UAM were employed to model the battery and validate its state estimator. (2) Additionally, the current sensor bias was estimated simultaneously with the SOC. Using the shunt resistor, an actual bias of around 400 mA was measured from the Hall sensor, equivalent to a 0.1 C-rate for the cell used in the experiment. The measured amount of bias is approximately the median of the values imagined by the prior studies: 10, 20 mA [11], 12.5, 25 mA [10], 100 mA [9], 113.5 mA [12], 500 mA [13], and 1000 mA [8]. Our model-based estimator corrected this Hall sensor bias, which enabled SOC estimation error to remain below 2% against the load profiles. Further improvement in SOC estimation is possible by achieving greater accuracy in predicting terminal voltage across the full range of SOCs. Additionally, SOC estimation can be affected due to changes in the total capacity, requiring it to be estimated correctly and updated periodically.

Author Contributions: Conceptualization, W.S. and J.-H.C.; methodology, M.Y.Y.; software, M.Y.Y. and J.H.L.; validation, M.Y.Y. and J.H.L.; investigation, J.H.L.; writing—original draft preparation, M.Y.Y.; writing—review and editing, W.S. and J.-H.C.; supervision W.S.; project administration, J.S.H.; funding acquisition, J.S.H. All authors have read and agreed to the published version of the manuscript.

Funding: This research was funded by the “Technology development of hybrid electric propulsion systems for manned future air mobility” program (1711170902) by Korea Aerospace Research Institute, Republic of Korea.

Conflicts of Interest: The authors declare no conflict of interest.

Appendix A

Non-linear system model and measurement function of the ESC model.

$$\begin{bmatrix} i_{R_1,k} \\ i_{R_2,k} \\ z_k \\ h_k \\ i_{b,k} \end{bmatrix} = \begin{bmatrix} e^{-\frac{\Delta t}{R_1 C_1}} & 0 & 0 & 0 & e^{-\frac{\Delta t}{R_1 C_1}} - 1 \\ 0 & e^{-\frac{\Delta t}{R_2 C_2}} & 0 & 0 & e^{-\frac{\Delta t}{R_2 C_2}} - 1 \\ 0 & 0 & 1 & 0 & \frac{\eta \Delta t}{Q} \\ 0 & 0 & 0 & e^{-|\frac{\eta(i_{k-1} - i_{b,k-1})\gamma \Delta t}{Q}|} & 0 \\ 0 & 0 & 0 & 0 & 1 \end{bmatrix} \begin{bmatrix} i_{R_1,k-1} \\ i_{R_2,k-1} \\ z_{k-1} \\ h_{k-1} \\ i_{b,k-1} \end{bmatrix} + \begin{bmatrix} 1 - e^{-\frac{\Delta t}{R_1 C_1}} & 0 \\ 1 - e^{-\frac{\Delta t}{R_2 C_2}} & 0 \\ -\frac{\eta \Delta t}{Q} & 0 \\ 0 & e^{-|\frac{\eta(i_{k-1} - i_{b,k-1})\gamma \Delta t}{Q}|} - 1 \\ 0 & 0 \end{bmatrix} \begin{bmatrix} i_{k-1} \\ \text{sign}(i_{k-1} - i_{b,k-1}) \end{bmatrix} + w_{k-1} \quad (\text{A1})$$

$$v_{T,k} = OCV(z_k) + M_0 \text{sign}(i_k) + M h_k - R_1 i_{R_1,k} - R_2 i_{R_2,k} - R_0(i_k - i_{b,k}) + v_k \quad (\text{A2})$$

State transition matrix \hat{A} , input matrix \hat{B} , output matrix \hat{C} , and feedthrough matrix \hat{D} derived for linear approximation.

$$\hat{A}_{k-1} = \begin{bmatrix} e^{-\frac{\Delta t}{R_1 C_1}} & 0 & 0 & 0 & e^{-\frac{\Delta t}{R_1 C_1}} - 1 \\ 0 & e^{-\frac{\Delta t}{R_2 C_2}} & 0 & 0 & e^{-\frac{\Delta t}{R_2 C_2}} - 1 \\ 0 & 0 & 1 & 0 & \frac{\eta \Delta t}{Q} \\ 0 & 0 & 0 & e^{-|\frac{\eta(i_{k-1} - i_{b,k-1})\gamma \Delta t}{Q}|} & \frac{\eta \gamma \Delta t}{Q} \{1 + \text{sign}(i_{k-1} - i_{b,k-1})h_{k-1}\} e^{-|\frac{\eta(i_{k-1} - i_{b,k-1})\gamma \Delta t}{Q}|} \\ 0 & 0 & 0 & 0 & 1 \end{bmatrix} \quad (\text{A3})$$

$$\hat{B}_{k-1} = \begin{bmatrix} 1 & 0 & 0 & 0 & 0 \\ 0 & 1 & 0 & 0 & 0 \\ 0 & 0 & 1 & 0 & 0 \\ 0 & 0 & 0 & 1 & 0 \\ 0 & 0 & 0 & 0 & 1 \end{bmatrix}$$

$$\hat{C}_k = \begin{bmatrix} -R_1 & -R_2 & \frac{\partial OCV(z_k)}{\partial z_k} & M & R_0 \end{bmatrix}$$

$$\hat{D}_k = 1$$

References

1. Ding, Y.; Cano, Z.P.; Yu, A.; Lu, J.; Chen, Z. Automotive Li-ion batteries: Current status and future perspectives. *Electrochem. Energy Rev.* **2019**, *2*, 1–28. [CrossRef]
2. Mauler, L.; Duffner, F.; Zeier, W.G.; Leker, J. Battery cost forecasting: A review of methods and results with an outlook to 2050. *Energy Environ. Sci.* **2021**, *14*, 4712–4739. [CrossRef]
3. EASA Certifies Electric Aircraft, First Type Certification for Fully Electric Plane World-Wide. Available online: <https://www.easa.europa.eu/newsroom-and-events/press-releases/easa-certifies-electric-aircraft-first-type-certification-fully> (accessed on 20 February 2023).
4. Batteries Systems and BMS. Available online: <https://www.pipistrel-aircraft.com/products/other-products/batteries-systems-and-bms> (accessed on 20 February 2023).
5. Mansour, I.; Frisk, E.; Jemni, A.; Krysander, M.; Liouane, N. State of charge estimation accuracy in charge sustainable mode of hybrid electric vehicles. *IFAC-Pap.* **2017**, *50*, 2158–2163. [CrossRef]
6. Zhang, S.; Zhang, J. Optimal state-of-charge value for charge-sustaining mode of plug-in hybrid electric vehicles. *IEEE Access* **2020**, *8*, 187959–187964. [CrossRef]
7. Sohn, J.; Sunwoo, M.; Min, K.; Shin, J.; Han, M. Power management strategy for the 48 V mild hybrid electric vehicle based on the charge-sustaining control. *Int. J. Automot. Technol.* **2019**, *20*, 37–49. [CrossRef]
8. Malysz, P.; Gu, R.; Ye, J.; Yang, H.; Emadi, A. State-of-charge and state-of-health estimation with state constraints and current sensor bias correction for electrified powertrain vehicle batteries. *IET Electr. Syst. Transp.* **2016**, *6*, 136–144. [CrossRef]
9. Zhao, S.; Duncan, S.R.; Howey, D.A. Observability analysis and state estimation of lithium-ion batteries in the presence of sensor biases. *IEEE Trans. Control Syst. Technol.* **2016**, *25*, 326–333. [CrossRef]

10. Al-Gabalawy, M.; Hosny, N.S.; Dawson, J.A.; Omar, A.I. State of charge estimation of a Li-ion battery based on extended Kalman filtering and sensor bias. *Int. J. Energy Res.* **2021**, *45*, 6708–6726. [[CrossRef](#)]
11. Bhattacharyya, H.S.; Choudhury, A.B.; Chanda, C.K. On-road estimation of state of charge of lithium-ion battery by extended and dual extended Kalman filter considering sensor bias. *Int. J. Energy Res.* **2022**, *46*, 15182–15197. [[CrossRef](#)]
12. He, J.; Feng, D.; Hu, C.; Wei, Z.; Yan, F. Two-layer online state-of-charge estimation of lithium-ion battery with current sensor bias correction. *Int. J. Energy Res.* **2019**, *43*, 3837–3852. [[CrossRef](#)]
13. Nguyen Van, C.; Nguyen Vinh, T. SOC estimation of the lithium-ion battery pack using a sigma point Kalman filter based on a cell's second order dynamic model. *Appl. Sci.* **2020**, *10*, 1896–1912. [[CrossRef](#)]
14. Plett, G.L. Extended Kalman filtering for battery management systems of LiPB-based HEV battery packs: Part 3. State and parameter estimation. *J. Power Sources* **2004**, *134*, 277–292. [[CrossRef](#)]
15. He, H.; Xiong, R.; Fan, J. Evaluation of lithium-ion battery equivalent circuit models for state of charge estimation by an experimental approach. *Energies* **2011**, *4*, 582–598. [[CrossRef](#)]
16. Farag, M.; Fleckenstein, M.; Habibi, S.R. Li-ion battery SOC estimation using non-linear estimation strategies based on equivalent circuit models. *SAE Int.* **2014**, *1*, 1–11.
17. Kai, W.; Xiao, F.; Jinbo, P.; Jun, R.; Chongxiang, D.; Liwei, L. State of charge (SOC) estimation of lithium-ion battery based on adaptive square root unscented kalman filter. *Int. J. Electrochem. Sci.* **2020**, *15*, 9499–9516. [[CrossRef](#)]
18. Hu, Y.; Yurkovich, S. Battery cell state-of-charge estimation using linear parameter varying system techniques. *J. Power Sources* **2012**, *198*, 338–350. [[CrossRef](#)]
19. Huang, Z.; Fang, Y.; Xu, J. Soc estimation of li-ion battery based on improved ekf algorithm. *Int. J. Automot. Technol.* **2021**, *22*, 335–340. [[CrossRef](#)]
20. Guo, Y.; Zhao, Z.; Huang, L. SoC estimation of lithium battery based on AEKF algorithm. *Energy Procedia* **2017**, *105*, 4146–4152. [[CrossRef](#)]
21. Su, J.; Strandt, A.; Schneider, S.; Yaz, E.; Josse, F. Improved State of Charge Estimation of Lithium-ion Battery cells. In Proceedings of the 2021 European Control Conference (ECC), Virtual Conference, 29 June–2 July 2021.
22. Kim, D.; Koo, K.; Jeong, J.J.; Goh, T.; Kim, S.W. Second-order discrete-time sliding mode observer for state of charge determination based on a dynamic resistance li-ion battery model. *Energies* **2013**, *6*, 5538–5551. [[CrossRef](#)]
23. Spagnol, P.; Rossi, S.; Savaresi, S.M. Kalman filter SoC estimation for Li-ion batteries. In Proceedings of the 2011 IEEE International Conference on Control Applications (CCA), Denver, CO, USA, 28–30 September 2011.
24. Lin, X. Analytic derivation of battery SOC estimation error under sensor noises. *IFAC-Pap.* **2017**, *50*, 2175–2180. [[CrossRef](#)]
25. Meng, J.; Stroe, D.I.; Ricco, M.; Luo, G.; Teodorescu, R. A simplified model-based state-of-charge estimation approach for lithium-ion battery with dynamic linear model. *IEEE Trans. Ind. Electron* **2018**, *66*, 7717–7727. [[CrossRef](#)]
26. Zhao, L.; Liu, Z.; Ji, G. Lithium-ion battery state of charge estimation with model parameters adaptation using H_∞ extended Kalman filter. *Control Eng. Pract.* **2018**, *81*, 114–128. [[CrossRef](#)]
27. Hu, X.; Sun, F.; Zou, Y. Estimation of state of charge of a lithium-ion battery pack for electric vehicles using an adaptive Luenberger observer. *Energies* **2010**, *3*, 1586–1603. [[CrossRef](#)]
28. Jiani, D.; Youyi, W.; Changyun, W. Li-ion battery SOC estimation using particle filter based on an equivalent circuit model. In Proceedings of the 2013 10th IEEE International Conference on Control and Automation (ICCA), Hangzhou, China, 12–14 June 2013.
29. Koirala, N.; He, F.; Shen, W. Comparison of two battery equivalent circuit models for state of charge estimation in electric vehicles. In Proceedings of the 2015 IEEE 10th Conference on Industrial Electronics and Applications (ICIEA), Auckland, New Zealand, 15–17 June 2015.
30. DHAB V2. Available online: <https://www.lem.com/en/product-list/dhab-s145> (accessed on 20 February 2023).
31. Yokogawa 2215 Series Shunts. Available online: <https://www.tek-ac.com/product/dcs/yokogawa-dcs/shunt/yokogawa-2215-series-shunts> (accessed on 20 February 2023).
32. Lecture Notes and Recordings for ECE4710/5710: Modeling, Simulation, and Identification of Battery Dynamics. Available online: <http://mocha-java.uccs.edu/ECE5710/index.html> (accessed on 20 February 2023).
33. Viberg, M. Subspace methods in system identification. *IFAC Proc. Vol.* **1994**, *27*, 1–12. [[CrossRef](#)]
34. lsqnonneg. Available online: <https://mathworks.com/help/matlab/ref/lsqnonneg.html> (accessed on 20 February 2023).
35. Extended Kalman Filter. Available online: https://en.wikipedia.org/wiki/Extended_Kalman_filter (accessed on 20 February 2023).

Disclaimer/Publisher's Note: The statements, opinions and data contained in all publications are solely those of the individual author(s) and contributor(s) and not of MDPI and/or the editor(s). MDPI and/or the editor(s) disclaim responsibility for any injury to people or property resulting from any ideas, methods, instructions or products referred to in the content.